

Durham Research Online

Deposited in DRO:

25 February 2015

Version of attached file:

Other

Peer-review status of attached file:

Peer-reviewed

Citation for published item:

Allanach, B.C. and Grellscheid, D. and Quevedo, F. (2002) 'Selecting supersymmetric string scenarios from sparticle spectra.', Journal of high energy physics., 2002 (05). 048.

Further information on publisher's website:

<http://dx.doi.org/10.1088/1126-6708/2002/05/048>

Publisher's copyright statement:

Additional information:

Use policy

The full-text may be used and/or reproduced, and given to third parties in any format or medium, without prior permission or charge, for personal research or study, educational, or not-for-profit purposes provided that:

- a full bibliographic reference is made to the original source
- a [link](#) is made to the metadata record in DRO
- the full-text is not changed in any way

The full-text must not be sold in any format or medium without the formal permission of the copyright holders.

Please consult the [full DRO policy](#) for further details.

Selecting Supersymmetric String Scenarios From Sparticle Spectra

B.C. Allanach¹, D. Grellscheid², F. Quevedo²

¹ *CERN Theory Division, CH-1211 Geneva 23, Switzerland*

² *DAMTP, CMS, Wilberforce Road, Cambridge CB3 0WA, UK*

ABSTRACT: We approach the following question: if supersymmetry is discovered, how can we select among different supersymmetric extensions of the Standard Model? In particular, we perform an analysis of the sparticle spectrum in low-energy string effective theories, asking which observables best distinguish various scenarios. We examine scenarios differing by the fundamental string scale and concentrate on GUT and intermediate scale models. We scan over four parameters (two goldstino angles, $\tan\beta$ and the gravitino mass) in each scenario, finding ratios of sparticle masses that provide the maximum discrimination between them. The necessary accuracy for discrimination is determined in each case. We find that the required accuracy on various sparticle mass ratios is at the few percent level, a precision that may be achieved in future linear colliders. We also map out phenomenologically viable regions of parameter space.

KEYWORDS: Supersymmetry Breaking, Beyond Standard Model, Supersymmetric Models.

Contents

1. Introduction	1
2. Soft SUSY Breaking Terms	3
2.1 Scalar masses	4
2.2 Gaugino masses	5
2.3 A-terms	5
3. Renormalization Group Analysis	6
3.1 Constraints	6
3.2 String scale boundary conditions	6
3.3 Sparticle spectra	7
3.4 Maps of parameter space	10
3.5 Discriminating ratios	12
3.6 Interpretation	17
4. Conclusions	20

1. Introduction

There is great expectation in the high energy physics community of the possibility of discovering evidence of low-energy supersymmetry (SUSY) during the next few years. The smoking-gun signatures of production and detection of super-partners could be observable at the Tevatron, the Large Hadron Collider and a future linear collider facility. If such signatures are detected, we may enter a new era of high energy physics with closer contact between fundamental theory and experiment. Since there are many supersymmetric models, the issue may then turn from discovering SUSY to selecting and eliminating the different supersymmetric models that have been proposed over the years. It is therefore useful to examine ways of comparing the different models. Experiments may start to give us information not only about particle content but also about the mechanism of SUSY breaking and (eventually) the messenger of this breaking.

Many argue that the best motivated models of low energy SUSY are those that can be derived from string theory. Even though there is a plethora of possible specific string models, we can attempt to perform a fairly model independent analysis using

some general string scenarios. There are several ways to parameterize these scenarios. In recent years it was realised that the underlying scale of a fundamental string theory can be different from the Planck scale of 10^{19} GeV if the observable fields are confined to a brane within a higher dimensional world. Since the size of the extra dimensions is not necessarily fixed in such a theory, we have the freedom to argue for different values of the string scale. Two such possibilities with several indications in their favour are the GUT scale $M_{GUT} \sim O(10^{16})$ GeV [1] and the intermediate scale of around $M_I = 10^{11}$ GeV [2, 3]. The GUT scale is favoured by the data in the MSSM-desert gauge unification picture [1]. The intermediate scale is motivated by a natural solution to the strong CP problem, the scale of neutrino masses [3] and a natural supersymmetry breaking scale in gravity mediated supersymmetry breaking scenarios. But in this case, assuming an MSSM-like low energy spectrum, the gauge couplings evolved from the data at the electroweak scale M_Z to M_I do not meet, contrary to the naive string prediction. One must address the issue of gauge unification in the intermediate scale models, and two possibilities have been identified: one possibility is to achieve precocious unification [3] through the inclusion of additional matter fields on top of the MSSM content. Explicit intermediate scale string models have sometimes exhibited the existence of such superfields extra to the MSSM [4]. Another possibility is mirage gauge coupling unification [5]. In this picture, gauge unification at the GUT scale is merely an illusion created by string loop effects; the field theoretic gauge couplings are set non-universally at the (intermediate) string scale. Here, no additional matter fields beyond the MSSM are necessary.

We can imagine having experimental data on supersymmetric particles and would like to see if they may be able to determine the favoured string scale, or other important parameters of the fundamental theory. In this way we would start to obtain relevant information about the fundamental theory at a large scale from measurements at low energies. Motivated by this possibility we ask to what extent we can discriminate scenarios for the underlying theory. See [6] for related work.

Supersymmetric phenomenology is extremely complicated. The sparticles undergo cascade decays which provide various signatures in experiments. Such signatures notoriously depend not only on the model of SUSY breaking, but also upon its parameters. If a SUSY breaking parameter changes, mass differences in the particle spectrum can change sign. Decay channels in the cascade particle decays then switch on and off, and the identified signature is easily lost. Such is the complexity of supersymmetric phenomenology that experimental studies of future colliders have typically focused on a few points in parameter space [7].

To avoid getting bogged down in such complexity and model dependence, and in order to start the phenomenology ball rolling, we will assume that some of the superparticles' masses have been measured. We will try to gain information on the high energy theory from their values. Explicitly, we will examine three different

scenarios:

- String scale at the GUT scale $M_{GUT} \sim O(10^{16})$ GeV, defined by the scale of electroweak gauge unification $g_1(M_{GUT}) = g_2(M_{GUT})$.
- Intermediate string scale ($M_I = 10^{11}$ GeV) with extra leptons to achieve gauge coupling unification at M_I , which we will refer to as *early unification*.
- Intermediate string scale ($M_I = 10^{11}$ GeV) with *mirage unification* [5]. The particle spectrum is assumed to be as in the MSSM, and the gauge couplings at M_I are unequal.

To predict sparticle masses from these scenarios, we must solve the renormalization group equations starting from a theoretical boundary condition parameterized by the string scale, the goldstino angles, $\tan \beta$ and the gravitino mass $m_{3/2}$. Constraints from experiments and cosmology (if a version of R -parity is conserved, as assumed here) restrict the models.

Previous studies have been performed on intermediate string-type scenarios. Two of the authors [8] previously mapped out the spectrum and naturalness parameter for the dilaton dominated scenario in the GUT, early unification and mirage scenarios. Baek *et al* extended this study to include bounds from $B \rightarrow X_s \gamma$, dark matter and $g-2$ of the muon [9]. The early unification spectrum and relic neutralino density has also been investigated [10] when one of the goldstino angles varies. However, the effects of moduli fields on the SUSY breaking was neglected in this study. Dark matter observables were also considered for mirage or early unification scenarios in ref. [11]. Dilaton domination (corresponding to a fixed limit of one of the goldstino angles) is in violation of a charge and colour breaking bound for GUT scale unification [12], but it was found that this bound does not restrict the intermediate scale case [8].

Here we extend previous investigations in three directions. Firstly, we scan over both of the goldstino angles. Secondly, we look for the combinations of sparticle mass measurements which provide the most discrimination between the string scenarios, once parameters are scanned over. Thirdly, we approach the question: is it possible to select a string scenario from a knowledge of the masses of the different sparticles? We re-phrase this question as: what accuracy in sparticle mass measurements is required to select a string scenario?

2. Soft SUSY Breaking Terms

The Type I string models considered here are based on orientifold compactifications of type IIB strings, and share a number of similarities with the well studied phenomenological models derived from compactified heterotic string theories [13]. Both contain a dilaton superfield S , and moduli fields T_i connected with the size and shape

of the extra dimensions. These two fields contribute to SUSY breaking when their auxiliary fields acquire vacuum expectation values (VEVs). We consider one overall modulus T and later one blowing-up mode M as a parameterization of the stringy SUSY breaking. The respective contribution of F^S and F^T to the SUSY soft breaking terms can be parameterized in a goldstino angle θ (where $\sin \theta = 1$ corresponds to dilaton domination and $\cos \theta = 1$ denotes moduli domination).

One difference between heterotic and type I string models is that the string scale is not constrained to be near the Planck mass. Furthermore, the set of moduli fields connected to the blowing-up modes, M_α , play a more relevant role for SUSY breaking in Type I models than in the heterotic ones. They contribute explicitly to the gauge kinetic coupling and therefore their F -terms may induce gaugino masses and the other soft breaking terms. M mixes in the Kähler potential with the modulus field T . Accordingly it is convenient to introduce a second, (F^T, F^M) mixing angle ϕ in analogy to the usual dilaton-moduli mixing angle θ . To summarise,

$$\begin{pmatrix} F^S \\ F^T \\ F^M \end{pmatrix} = \begin{pmatrix} \sin \theta \\ \cos \theta \sin \phi \\ \cos \theta \cos \phi \end{pmatrix} F_{total}, \quad (2.1)$$

where $F_{total} = \sqrt{F_S^2 + F_T^2 + F_M^2}$.

The introduction of θ and ϕ provides a convenient way to parameterize the influence which the various VEVs have on the soft terms. We will generalise the results of ref. [8] where only the dilaton domination case was considered extensively. Here, we examine a wider θ and ϕ range but leave out $\theta < 10^\circ$. For such small values of θ , the string-induced high scale boundary conditions on the soft breaking terms reach a similar magnitude as the one-loop order anomaly mediated SUSY breaking terms, which therefore cannot be neglected. The complete set of soft breaking terms of combined anomaly and gravity mediation has not yet been computed [14]. We therefore leave this slice of parameter space to the future, when such terms might be included in an analysis. Like the analysis in [8], we assume that the full standard model gauge group arises from a single brane and that SUSY breaking is dominated by the F terms of the S , T and M fields. This results in the following soft breaking terms in the $T + \bar{T} \rightarrow \infty$ limit:

2.1 Scalar masses

All scalar masses receive the universal soft SUSY breaking term

$$m_0^2 = V_0 + m_{3/2}^2 \left(1 - \frac{3}{k} C^2 \cos^2 \theta \sin^2 \phi \right) + \mathcal{O} \left(\frac{1}{(T + \bar{T})^2} \right), \quad (2.2)$$

where $C = \sqrt{1 + \frac{V_0}{3m_{3/2}^2}}$, and V_0 is the vacuum energy. k depends on the form of the

Kähler potential and can be set constant¹ [8]. We set $k = 3$ in this article, which avoids negative scalar mass squared values at the string scale. Higher values of k are possible, this would lead to a weaker dependence of the scalar soft masses on the goldstino angles. As usual we will take $C = 1$ corresponding to $V_0 = 0$, *i.e.* a vanishing cosmological constant.

2.2 Gaugino masses

The gaugino masses are equal to

$$M_a = \sqrt{3}Cm_{3/2}\frac{\alpha_a}{\alpha_{\text{GUT}}}\left(\sin\theta - \frac{s_a}{8\pi}\alpha_{\text{GUT}}\cos\theta\left(\frac{\delta_{\text{GS}}}{\sqrt{k}}\sin\phi + \cos\phi\right)\right) + \mathcal{O}\left(\frac{1}{(T+\bar{T})^2}\right). \quad (2.3)$$

Here δ_{GS} is the Green-Schwarz term coming from anomaly cancellation (like in compactified heterotic string models). Its value is a model dependent negative integer of order $\mathcal{O}(-10)$. We will fix its value to -10 from here on². Note that, in general, the gaugino masses have a non-universal boundary condition at the string scale. If the string scale is intermediate, $\alpha_{a=1,2,3} \neq \alpha_{\text{GUT}}$ provides non-universality in equation (2.3) from the first term. The second term provides non-universality at the string-scale through one-loop stringy effects away from the dilaton dominated limit ($\theta = 90^\circ$). This term is proportional to the model-dependent parameters s_a . In order to make mirage unification possible, $s_a = 2\pi\beta_a$ was chosen [5], where β_a are the usual MSSM renormalization β -function coefficients $(33/5, 1, -3)$.

2.3 A-terms

Under the assumption that the Yukawa couplings are moduli-independent, the trilinear couplings are

$$A_{\alpha\beta\gamma} = -\sqrt{3}Cm_{3/2}\left(\sin\theta + \cos\theta\cos\phi\hat{K}'\right) + \mathcal{O}\left(\frac{1}{(T+\bar{T})^2}\right). \quad (2.4)$$

Here $\hat{K} = \hat{K}(M + M^* - \delta_{\text{GS}}\log(T + T^*))$, the M - and T -dependent part of the Kähler potential. One can set $\hat{K}' = 0$ [8], since all fields are assumed to be in the minimum of the potential, for which the argument of \hat{K} vanishes.

¹Usually in heterotic models the scalar masses are non-universal, since the coefficient of $\cos^2\theta$ depends on the so-called modular weights of the corresponding matter fields [15, 13]. If we considered several T fields here, we could also expect a non-universal behaviour, parameterized by different values of the constant k . However, for a single T field we get the universal behaviour shown in (2.2), which amounts to saying that in these models all matter fields have modular weight -1 . For a recent discussion of non-universal soft terms in a different context, see for instance [16].

²Different values for δ_{GS} affect the dependence of M_a on the goldstino angle ϕ . While this is negligible for $|\delta_{\text{GS}}| \lesssim \frac{1}{\alpha_{\text{GUT}}}$ where the minimum of M_a stays very close to $\theta = 0$ on the (θ, ϕ) plane, higher values of δ_{GS} lead to a significant perturbation away from $\theta = 0$. For a discussion of variable δ_{GS} , see [17].

3. Renormalization Group Analysis

In order to analyse the sparticle spectra we use the ISASUGRA part of the ISAJET 7.51 package [18] to obtain the SUSY spectrum starting from the high-energy boundary conditions detailed above.

3.1 Constraints

We use the following experimental constraints to limit the scenarios [19, 20]:

$$m_{\tilde{\chi}_1^0} > 45 \text{ GeV} \quad m_{\tilde{\chi}_1^\pm} > 103 \text{ GeV} \quad m_{h_0} > 113.5 \text{ GeV}. \quad (3.1)$$

We will also use constraints from the recently measured muon anomalous magnetic moment $a_\mu = (g - 2)/2$. The experiment E821 at Brookhaven National Laboratory (BNL) reported the measurement [21]

$$a_\mu = (11659202 \pm 14 \pm 6) \times 10^{-10}. \quad (3.2)$$

The precision in the measurement already significantly constrains the SUSY parameter space and will improve in the future. We will constrain all investigated models to be within 90% CL of the central value of the measurement [22], *i.e.*

$$-4.2 \times 10^{-10} < \delta a_\mu < 41.3 \times 10^{-10}. \quad (3.3)$$

The final constraint is the absence of a charged lightest supersymmetric particle (CLSP). This constraint must be applied when the LSP is stable on cosmological time scales. This is the case here because we implicitly assume that a version of R -parity holds, as recently found in specific string models [23].

3.2 String scale boundary conditions

As mentioned above, we consider three overall scenarios: GUT scale unification (with the string scale set to $M_S = 2 \times 10^{16}$ GeV), early unification and mirage unification (both with $M_S = M_I = 1 \times 10^{11}$ GeV). The MSSM spectrum is assumed in each case, except for early unification where $2 \times L_L + 3 \times E_R$ vector-like representations are added to the MSSM in order to achieve gauge unification at M_I [8]. It is assumed that these extra representations have negligible Yukawa couplings. We add their effect to the MSSM gauge β -functions above 1 TeV.

The string-scale boundary conditions on the soft terms were obtained from equations (2.2-2.4), with $m_{3/2}$, θ and ϕ , as well as $\tan \beta$ as free parameters. Throughout the whole analysis $\mu > 0$ and $m_t = 175$ GeV were assumed [19]. Negative μ leads to a negative δa_μ , which is limited from equation 3.3 to be small in magnitude. This means that, for a given value of $\tan \beta$, the sparticles must be heavy in order to suppress their contribution to δa_μ (compare figs. 3 and 4). In this limit, effects of the sign of μ upon the mass spectrum are suppressed. We can therefore safely ignore the

	θ	ϕ	$m_{3/2}$	$\tan\beta$	μ	m_t	V_0	C	k	δ_{GS}	M_{GUT}	M_I
range	10-90°	0-90°	50-1500	2-50	> 0	175	0	1	3	-10	2×10^{16}	10^{11}

Table 1: Summary of parameters. The first four parameters are scanned over, and their range is detailed. For the others, their value is kept constant except for μ which is constrained to give the correct value of M_Z . All massive parameters ($m_{3/2}, m_t, M_I, M_{\text{GUT}}$) are given in units of GeV.

$\mu < 0$ case because its resulting spectra will be included in our $\mu > 0$ results. This also means, though, that the sign of μ cannot be determined from these spectra, unless the sparticles are too light to be compatible with $\mu < 0$ for any $\tan\beta$.

In the GUT case, $\alpha_a = \alpha_{\text{GUT}} = 1/25$ was used in equation (2.3) for all gauge groups $a = 1, 2, 3$. In the mirage unification case, however, the gauge couplings only *appear* to unify at the GUT scale. In reality they are set at the intermediate scale $M_I = 10^{11}$ GeV to non-universal values³. In our analysis,

$$\alpha_1(M_I) = \frac{1}{37.6}, \quad \alpha_2(M_I) = \frac{1}{27.0}, \quad \alpha_3(M_I) = \frac{1}{19.8} \quad (3.4)$$

is the set of values which remains reasonably stable under iterations of inserting them into equation (2.3) and running the RGEs again.

For each of the three scenarios that we consider, we scan over the free parameters $\theta, \phi, \tan\beta$ and $m_{3/2}$. $\theta = 90^\circ$ corresponds to the dilaton domination case considered in [8], and the SUSY soft mass terms are independent of ϕ in this case. As mentioned above, values of $\theta < 10^\circ$ were not considered, since in this case tree level soft masses would vanish and it would not be possible to neglect the one-loop effects from anomaly mediated SUSY breaking, which might modify the soft terms considerably. Table 1 shows the default ranges and increments of scanned parameters. It also summarises the other parameters that were kept constant. When different values were used for a plot, we will mention it explicitly.

3.3 Sparticle spectra

In order to get some feeling for the effect of the goldstino angles, we first illustrate their effect upon the sparticle spectra. We choose the mirage unification scenario as a first example. The other scenarios do differ from these spectra quantitatively, but the effect of the goldstino angles is similar in each case. In figure 1, we show the variation of the mirage unification spectrum with θ for $\tan\beta = 30$, $m_{3/2} = 300$ GeV and $\phi = 60^\circ$. As mentioned above, $\theta = 90^\circ$ corresponds to the dilaton dominated limit. From the figure, we see that larger θ increases the splittings between sparticles. Larger θ corresponds to larger gaugino masses in eq. (2.3) and the larger gluino mass

³We note that ref. [8] assumes gaugino universality, which leads to different conclusions for the mirage scenario, especially for the charged LSP constraints.

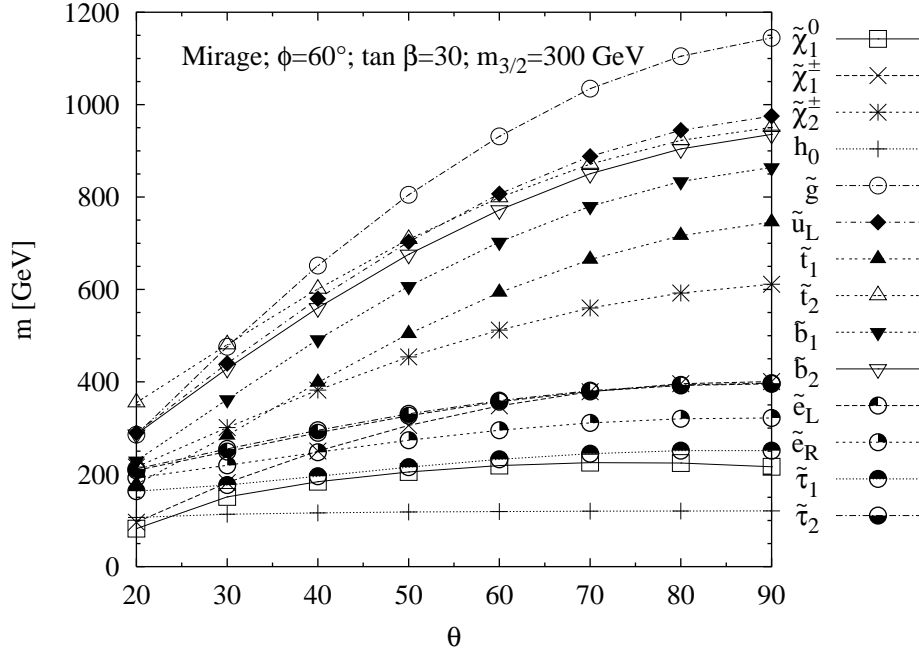


Figure 1: Variation of mirage unification particle mass spectrum with θ . We use $\phi = 60^\circ$, $\tan \beta = 30$ and $m_{3/2} = 300$ GeV. The key on the right-hand side of the figure details the flavour of particle.

raises the other coloured particle masses in the running from M_I to M_Z . The weak gauginos also show a milder change from the larger values of $M_{1,2}$. Sleptons are largely unaffected by the variation of θ , demonstrating the fact that the mild increase in m_0 in eq. (2.2) from increasing θ is a relatively minor effect.

The ordering of superparticle masses is largely unaffected by changes in θ , except for the lightest chargino, which crosses the $\tilde{e}_R, \tilde{\tau}_2$ and \tilde{e}_L lines⁴ and the lightest stop, which crosses the heavier chargino line. Each ordering can correspond to different cascade decay channels, and might be used to restrict θ once these decays are observed. For example, when the chargino crosses the \tilde{e}_R line, nothing much changes because the lightest chargino does not have significant couplings to right-handed selectrons. However, decays into neutrinos and \tilde{e}_L or $\tilde{\tau}_2$ (which can have a significant left-handed component for large $\tan \beta$) become viable for $\theta > 70^\circ$.

In figure 2a, we show the variation of the mirage unification particle spectrum with ϕ for $\tan \beta = 30$, $m_{3/2} = 300$ GeV and $\theta = 30^\circ$. Here, increasing ϕ has a smaller effect than θ , but generally decreases the splittings between sparticle masses. The effect is relatively small because the gaugino masses are only sensitive to ϕ through a suppression factor in eq. (2.3). Most of the particle masses decrease with increasing ϕ , except for the lightest neutralino (which becomes heavier) and the lightest chargino (which remains roughly constant). This can be understood by

⁴It is difficult to discern in the figure that the $\tilde{\tau}_2$ and \tilde{e}_L are quasi-degenerate.

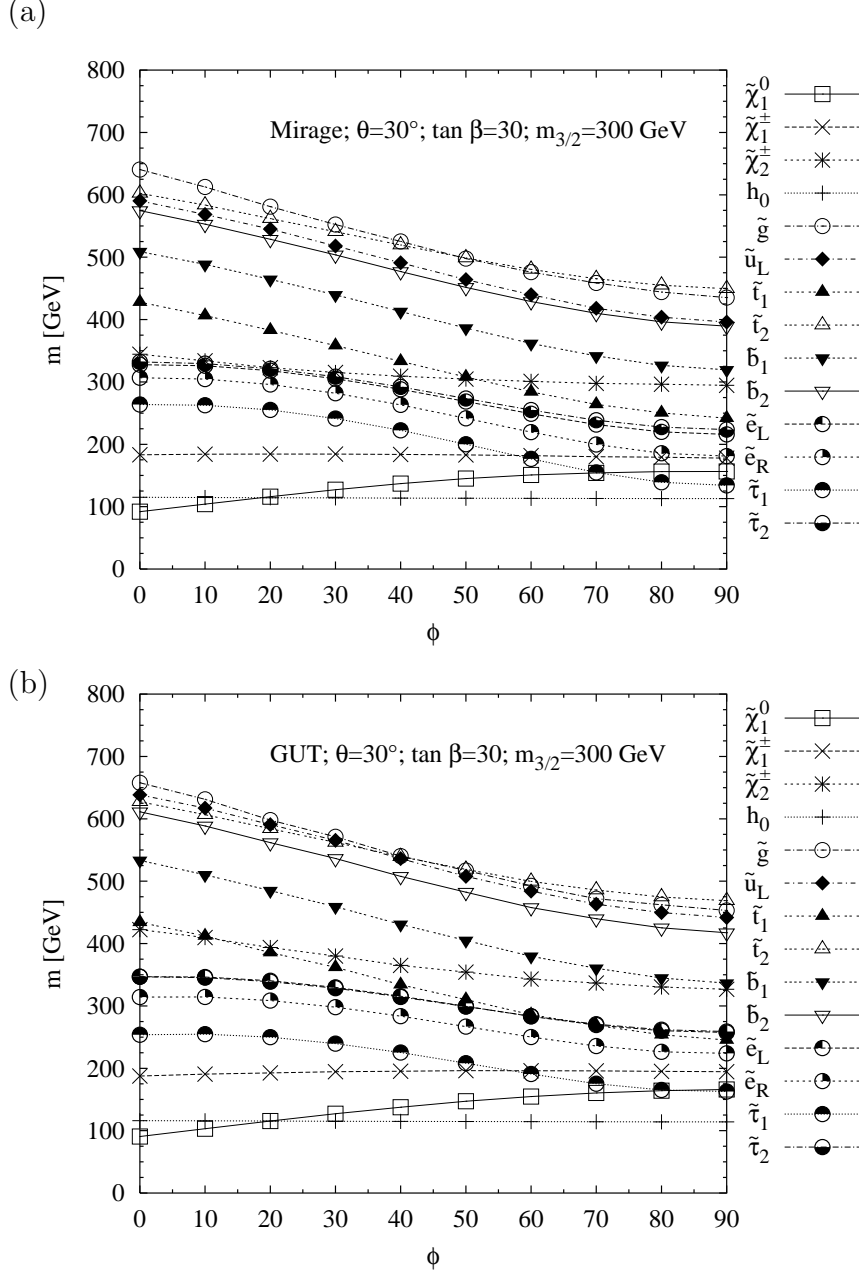


Figure 2: Variation of sparticle mass spectrum with ϕ for (a) mirage and (b) GUT-scale unification scenarios. We use $\theta = 30^\circ$, $\tan \beta = 30$ and $m_{3/2} = 300$ GeV. The key on the right-hand side of the figure details the flavour of sparticle.

considering the effect of increasing ϕ on the scalar masses in eq. (2.2). The figure shows that the model would be ruled out for $\phi \geq 70^\circ$ because of a stau LSP. Aside from this, important changes in the ordering of sparticle masses occur between the lightest stau and chargino and the heavier chargino and the lightest stop. The heavier stop becomes heavier than the gluino for $\phi > 50^\circ$. This is potentially important because future e^+e^- machines can produce and measure gluinos more easily through

the decays of pair-produced squarks. In this example, however, the mass difference between gluino and the heavier stop is not sufficient to produce an on-shell top quark in a decay. Thus such a process would be highly phase-space suppressed.

Figure 2b shows the variation of the GUT scale unification sparticle spectrum with ϕ for $\tan\beta = 30$, $m_{3/2} = 300$ GeV and $\theta = 30^\circ$. While quantitative differences exist between figures 2a and 2b, it is clear that the two spectra are qualitatively very similar. There is, however, some re-ordering of sparticle masses between the GUT-scale and mirage-scale scenarios for certain values of ϕ . For example, at $\phi = 20^\circ$, the heavy chargino and light stop are interchanged. It would be difficult to discriminate the two scenarios on the basis of decays implying a certain ordering of the lightest stop and chargino since there is no *a priori* information about ϕ , although it might be possible to fit the masses to certain values of θ, ϕ if the experimental accuracy were good enough. For larger values of θ , the variation of the spectrum with ϕ significantly decreases because the terms that depend upon it in the boundary conditions eqs. (2.2)-(2.4) become smaller and sub-dominant to the other θ dependent terms.

3.4 Maps of parameter space

We now explore the parameter space, including constraints from the sparticle mass limits in eq. (3.1), requiring that the $g-2$ anomalous magnetic moment be within 90% CL of the central measured value, requiring correct electroweak symmetry breaking and imposing a neutral LSP. In figure 3, we present viable regions of $\tan\beta$ - $m_{3/2}$ parameter space for various points in the goldstino angle space and $\mu > 0$. Dilaton domination has been well covered in the literature [8, 9] and so we present other more general regions of the parameter space alongside the dilaton dominated limit in figure 3b. We see from the variation in the viable regions from figures 3a-3d that they are dependent upon the goldstino angles, which vary between each of the figures. For $\theta = 30^\circ$ and $\phi = 30^\circ$, we see from figure 3a that there is little dependence of the viable region upon the scenario assumed. The other three figures show a larger difference between the three scenarios, apart from for $\phi = 60^\circ, \theta = 30^\circ$, which does not distinguish the GUT and mirage unification regions significantly, as can be seen from fig. 3c. In figure 4, we show the available parameter space for $\mu < 0$. By comparing figs. 3 and 4, we see that $\mu < 0$ admits less parameter space. This is because the $g-2$ constraint restricts sparticles to be heavy for $\mu < 0$ in order to give a small contribution to the magnitude of the anomalous moment. The lower bounds upon sparticle masses are much stronger for high $\tan\beta$, where the contributions to the anomalous moment are largest. Figure 4 illustrates that (for low $\tan\beta$), there is a lower bound $m_{3/2} \gtrsim 400$ GeV.

There are often also bounds upon $\tan\beta$. Low $\tan\beta$ is ruled out by the direct lower bound upon the Higgs mass from LEP2 [19], whereas high $\tan\beta$ is either ruled out by the constraint of a neutral LSP, or of not too *large* a supersymmetric contribution

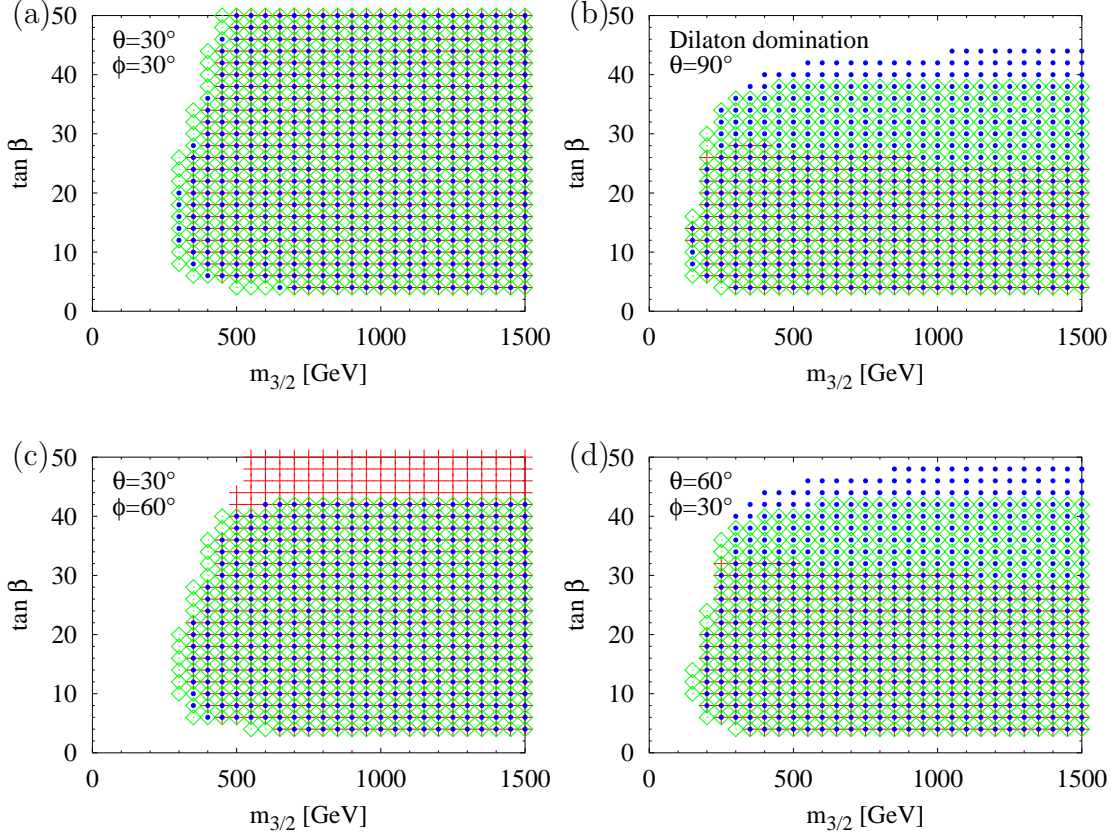


Figure 3: $\mu > 0$ maps of parameter space for the early unification (red crosses), mirage (blue dots) and GUT unification scale (green diamonds) scenarios. Here, we plot viable regions of $\tan\beta$ - $m_{3/2}$ parameter space for fixed values of the goldstino angles, after all exclusion limits were applied: (a) $\theta = 30^\circ$, $\phi = 30^\circ$, (b) $\theta = 90^\circ$, $\phi = \text{arbitrary}$, (c) $\theta = 30^\circ$, $\phi = 60^\circ$, (d) $\theta = 60^\circ$, $\phi = 30^\circ$.

to $g - 2$ of the muon. For instance in the dilaton domination $\mu > 0$ ($\mu < 0$) case we can see that the GUT scale scenario restricts $\tan\beta < 40$ (44), the early unification scenario requires $\tan\beta < 30$ (28) and mirage unification constrains $\tan\beta < 46$. For the lower value of $\theta = 30^\circ$ in the $\mu > 0$ case, the $\tan\beta$ bound disappears for $\phi = 30^\circ$ in all scenarios as in figure 3a, but reappears for higher $\phi = 60^\circ$ in the early and GUT-scale unification scenarios (figure 3d).

In figures 5a and 5b, we show the viable regions in goldstino angle space for fixed $m_{3/2} = 400$ GeV and $\tan\beta = 20, 40$ respectively. For lower $\tan\beta = 20$, there are viable dilaton-dominated cases for each scenario. However, for $\tan\beta = 40$ in figure 5b, dilaton domination ($\theta = 90^\circ$) is not viable except for the mirage unification case. The bounds $\phi \leq 50^\circ$ and $\theta < 70^\circ, 60^\circ$ apply to the GUT-scale and early unification scenarios respectively. For $\phi = 0^\circ$, there is still a large contribution to unification-scale sparticle masses from terms involving θ , so a lower bound on ϕ does

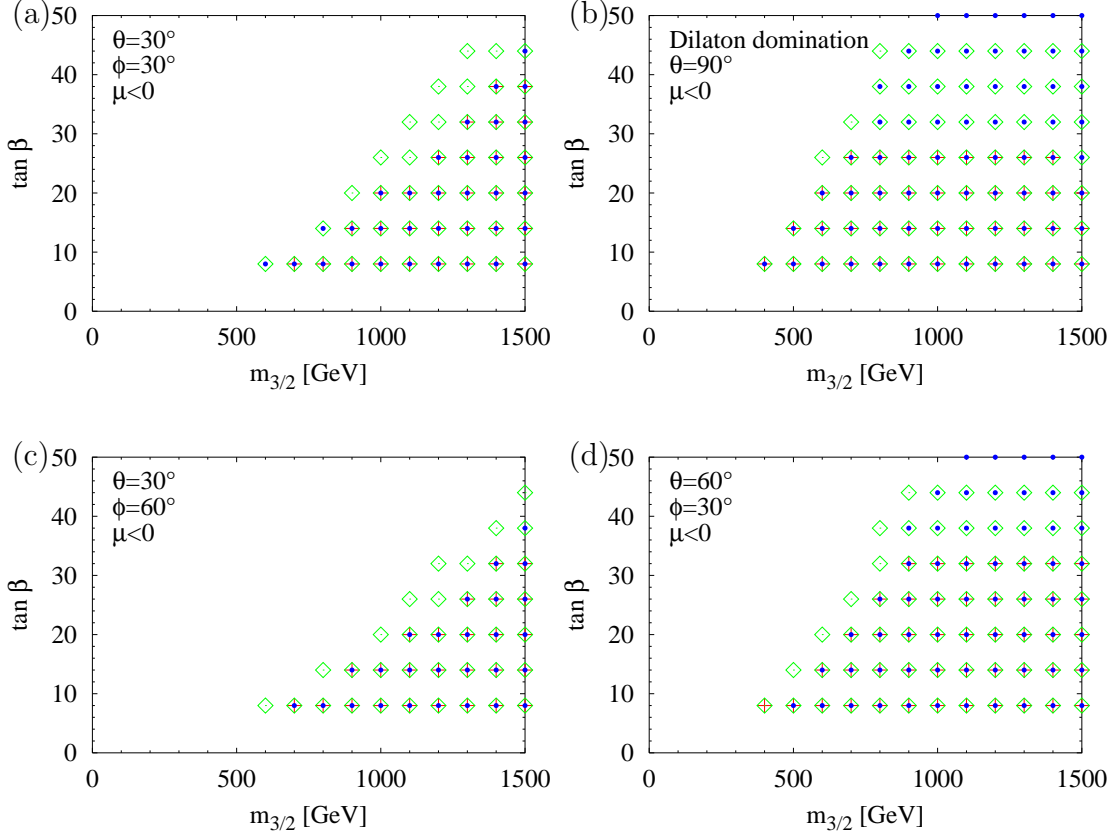


Figure 4: $\mu < 0$ maps of parameter space for the early unification (red crosses), mirage (blue dots) and GUT unification scale (green diamonds) scenarios. Here, we plot viable regions of $\tan \beta$ - $m_{3/2}$ parameter space for fixed values of the goldstino angles, after all exclusion limits were applied: (a) $\theta = 30^\circ$, $\phi = 30^\circ$, (b) $\theta = 90^\circ$, $\phi = \text{arbitrary}$, (c) $\theta = 30^\circ$, $\phi = 60^\circ$, (d) $\theta = 60^\circ$, $\phi = 30^\circ$.

not exist for general θ from particle mass bounds.

3.5 Discriminating ratios

We have searched through ratios of masses of sparticles to see which ones provide the largest discrimination between the three scenarios examined. The ideal situation would be to find ratios that are predicted to be completely disjoint regions for the three scenarios. Then, if the mass ratios were determined in an experiment, a comparison with these disjoint regions should reject or confirm one scenario. In general, this may not be possible so we resort to finding ratios which discriminate between some of the scenarios in some cases. Where disjoint regions are found, we will focus on the accuracy required in any mass ratio measurement that would be enough to discriminate two scenarios. This accuracy we will define as follows: supposing the central value of a measurement of a ratio lies on the edge of one of the regions. The fractional accuracy in each direction that would exclude each of the other scenarios

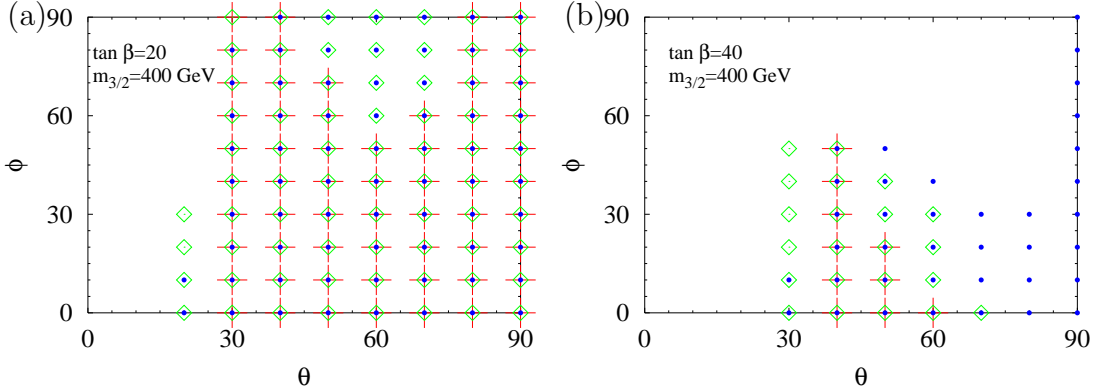


Figure 5: Maps of parameter space for the early unification (red crosses), mirage (blue dots) and GUT unification scale (green diamonds) scenarios. Here, we plot viable regions of θ - ϕ parameter space for fixed values of $m_{3/2}$ and $\tan\beta$: (a) $m_{3/2} = 400$ GeV, $\tan\beta = 20$, (b) $m_{3/2} = 400$ GeV, $\tan\beta = 40$

is taken. Then, we examine all points lying within a region and quote the lowest fractional accuracy on each ratio required to separate the regions. One ratio on its own does not provide enough separation once the parameters in each scenario are scanned over; we therefore resort to considering combinations of two ratios in order to see if the regions of each scenario are separated in two dimensional ratio space.

There are a few combinations of ratios that provide near separation. We display the best two such combinations in figure 6. For each point in the parameter scan described in table 1, that satisfies the constraints in eq. (3.1) as well as the neutral LSP constraint, one point appears on the plot. Here, we have taken input parameters *at random* within the ranges defined in table 1 for 10000 points (as is the case for the rest of this subsection). Each of the three scenarios were scanned over and shown on the plots. We have separated figure 6 into two cases: either the squark flavours/handedness are known, as assumed in figure 6a, or a squark mass averaged over the first two generations and handedness is used,

$$m_{\tilde{q}_{avg}} \equiv \frac{1}{8} (m_{\tilde{u}_L} + m_{\tilde{u}_R} + m_{\tilde{c}_L} + m_{\tilde{c}_R} + m_{\tilde{d}_L} + m_{\tilde{d}_R} + m_{\tilde{s}_L} + m_{\tilde{s}_R}), \quad (3.5)$$

as in figure 6b. For our numerical analysis we assumed degeneracy between the first two families, and therefore in all our figures, $m_{\tilde{u}_L}$ and $m_{\tilde{d}_L}$ can also stand for $m_{\tilde{c}_L}$ and $m_{\tilde{s}_L}$ respectively. The reason for showing both figures is the differing ability of hadron and lepton collider machines. It will be impossible for a hadron machine like the LHC to distinguish between the flavour of the almost-degenerate first two families of squarks. It is also difficult to see how a mass measurement of different handedness of squarks might occur. The third family typically are split from these in mass, and have additional heavy flavour tagging identification for their decay products and so

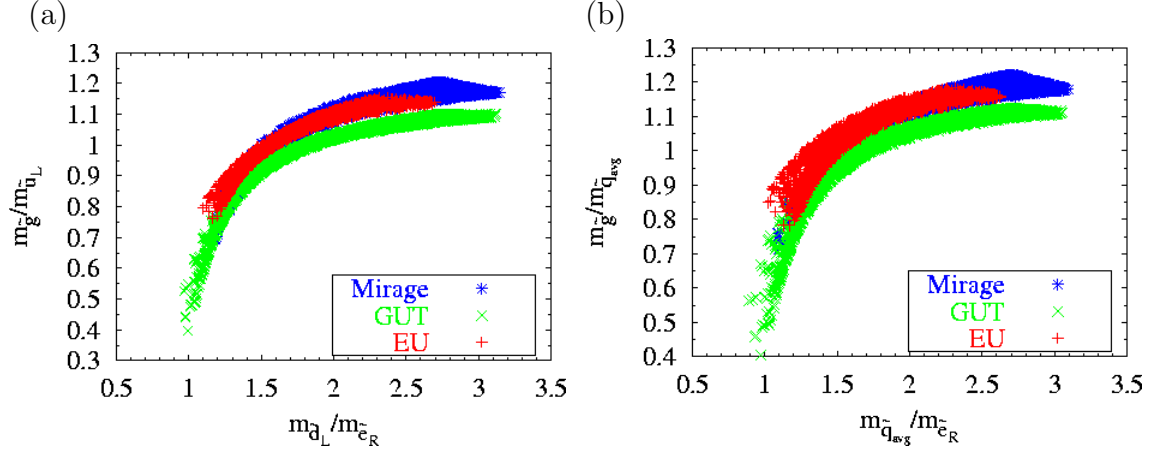


Figure 6: Highly discriminating ratios of sparticle masses. Each plotted point corresponds to one data point in four-dimensional parameter space $(\theta, \phi, \tan \beta, m_{3/2})$ that is not excluded by the imposed limits. In (b), $m_{\tilde{q}_{avg}}$ is as defined in the text. Pluses correspond to the early unification scenario, crosses to GUT-scale unification and stars to mirage unification.

it should be possible to separate these. On the other hand, possible future linear e^+e^- colliders are expected [24] to provide very precise measurements of $m_{\tilde{e}_L}$ and $m_{\tilde{e}_R}$. Because a future linear collider could scan to an energy that is sufficient to produce a particular mass of squark, it will be possible to separate up-type from down-type squarks provided there is enough energy to produce them, and identify which type squarks are produced from their cross-section. Handedness could either be determined by examining the decay chains, or by using polarised beams to favour production of one handedness or another. It is conceivable that squarks will only be produced at the LHC, and are too heavy for a particular linear collider facility to produce. It is for this reason that we provide discrimination plots for both individual and averaged squark masses. The importance of possessing individual squark mass measurements can then be assessed.

In figure 6a there is a large overlap between the early unification and mirage scenarios' predictions in the range $0.75 < m_{\tilde{g}}/m_{\tilde{u}_L} < 1.15$, but outside of this range separation is possible. GUT-scale unification can usually be discriminated from the other two scenario ranges, provided we measure the mass ratios with 1% accuracy. In Fig. 6b, we see that the effect of averaging over the squark mass measurements is to significantly decrease the discrimination between the mirage and GUT unification scenarios. There is significant overlap in the allowed ranges for all three scenarios, but that there are also regions of predicted mass ratios which can be only consistent with one particular scenario towards the bottom-left or top-right of the plot. If the empirical uncertainties on mass ratios are small enough and the underlying model

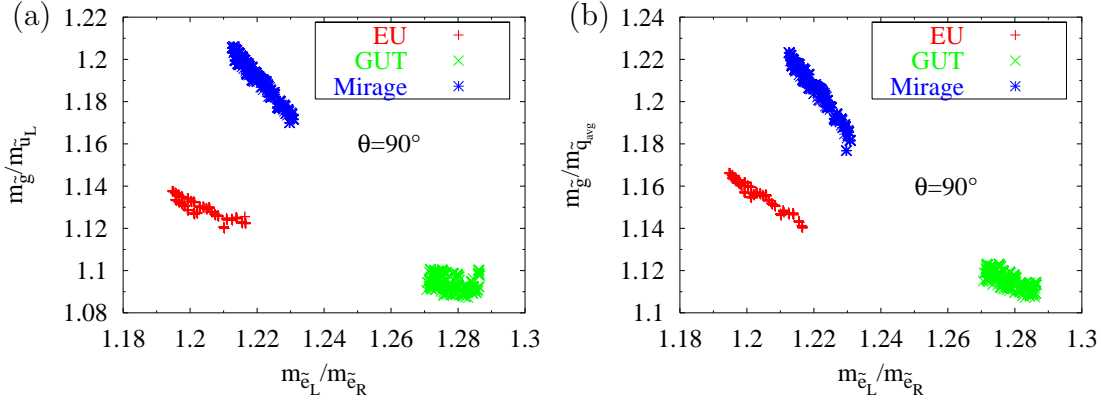


Figure 7: Highly discriminating ratios of sparticle masses for dilaton domination ($\theta = 90^\circ$). Each plotted point corresponds to one $(m_{3/2}, \tan \beta)$ -pair in the scan not excluded by any limits. Green crosses are predicted by the GUT unification scale, early unification is denoted by red crosses, and blue stars are valid for the mirage unification scenario.

does not lie in an overlap region, the correct scenario would be selected over the other two.

It is possible that other measurements (for example measuring Higgs couplings) will constrain some of the parameters of the model. For this reason, we will now assume that two of the four variables θ , ϕ , $\tan \beta$ or $m_{3/2}$ are constrained in order to see the resulting improvement in string scenario discrimination. An obvious example to examine is the dilaton domination scenario (corresponding to $\theta = 90^\circ$), which has attracted attention in the past in its own right. In figure 7a, we plot the ratios of masses $x \equiv m_{\tilde{e}_L}/m_{\tilde{e}_R}$ against $y \equiv m_{\tilde{g}}/m_{\tilde{u}_L}$ in the dilaton domination limit for all scanned values of the gravitino mass and $\tan \beta$ in table 1. We can clearly distinguish between the three scenarios because there is no overlap in their regions in ratio parameter space. From the figure, we note that at least a⁵ 3% measurement of $m_{\tilde{g}}/m_{\tilde{u}_L}$ and a 4% measurement in $m_{\tilde{e}_L}/m_{\tilde{e}_R}$ would be required to always separate the models on the basis of these ratios alone. This is a very positive result: assuming dilaton domination, we have complete discrimination. Figure 7b shows that there are minimal changes if one averages over the first two generations of squarks. The discriminating accuracy becomes smaller: 1% and 3% in $m_{\tilde{g}}/m_{\tilde{q}_{avg}}$ and $m_{\tilde{e}_L}/m_{\tilde{e}_R}$ respectively.

Figure 8 illustrates departures from dilaton domination. $m_{3/2}$ and $\tan \beta$ have been fixed in the figure, whereas θ and ϕ have been scanned over as in table 1. The figure shows the variation of the ratios $m_{\tilde{e}_R}/m_{\tilde{g}}$ and $m_{\tilde{q}_{avg}}/m_{\tilde{g}}$ as well as the variation of $m_{H^0}/m_{\tilde{b}_2}$ and $m_{A^0}/m_{\tilde{t}_2}$ with string scenario. Figures 8a and 8b have $\tan \beta = 30$ and $m_{3/2} = 250$ GeV fixed to different values than figures 8c and 8d ($\tan \beta = 6$ and

⁵We always quote the fractional uncertainty, *e.g.* on a ratio R , we quote the error required upon $\Delta R/R$.

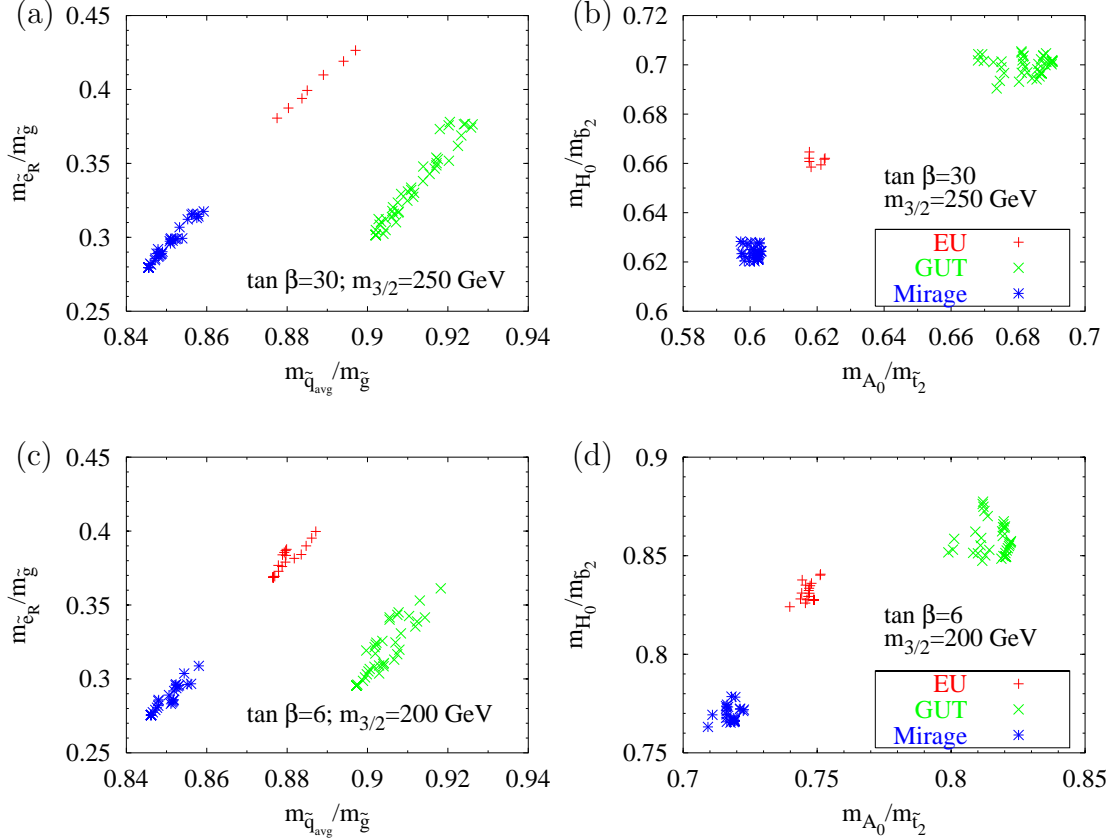


Figure 8: Highly discriminating ratios of sparticle masses for (a), (b): $\tan \beta = 30$, $m_{3/2} = 250$ GeV and (c), (d): $\tan \beta = 6$, $m_{3/2} = 200$ GeV. Each plotted point corresponds to one (θ, ϕ) -pair in the scan not excluded by the bounds. Green crosses are predicted by the GUT unification scale, early unification is denoted by red crosses, and blue stars are valid for the mirage unification scenario.

$m_{3/2} = 200$ GeV), in order to illustrate how the required discrimination accuracy can depend upon the supposedly constrained parameters. Discrimination is shown to generally be achieved for errors smaller than 14% in $m_{\tilde{e}_R}/m_{\tilde{g}}$ and 4% in $m_{\tilde{q}_{avg}}/m_{\tilde{g}}$ from figure 8a. These numbers happen to be roughly identical for a different choice of $\tan \beta$ and $m_{3/2}$, as shown in figure 8c. Figures 8b,d show how discrimination could be achieved with 5,7% errors respectively on $m_{H^0}/m_{\tilde{b}_2}$ and $m_{A^0}/m_{\tilde{t}_2}$. We note that the overall values of these two ratios in any one scenario depends sensitively upon the values of $\tan \beta$ and $m_{3/2}$. $\tan \beta$ and $m_{3/2}$ could then be constrained by their measurement.

We now fix the goldstino angles, to see if it is possible to distinguish the models when they are scanned over $m_{3/2}$ and $\tan \beta$. The usefulness of combinations of ratios of sparticle masses depends in general upon the value of these fixed goldstino angles. As figures 9a-9b show, however, that the required accuracy on the ratios $m_{\tilde{q}_{avg}}/m_{\tilde{g}}$ and $m_{\tilde{e}_R}/m_{\tilde{g}}$ does vary with respect to a variation of the goldstino angles.

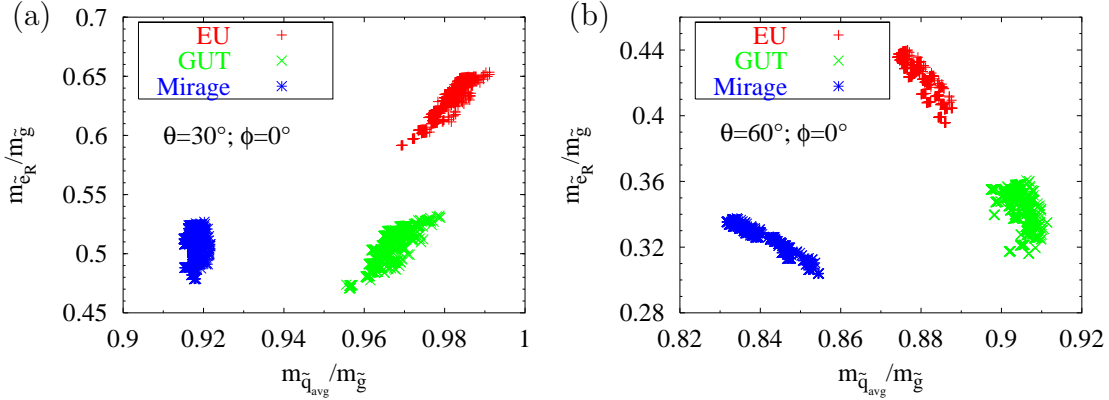


Figure 9: Discriminating ratios of sparticle masses in departures from dilaton domination: (a) $\theta = 30^\circ, \phi = 0^\circ$ and (b) $\theta = 60^\circ, \phi = 0^\circ$. Each plotted point corresponds to one $(m_{3/2}, \tan \beta)$ pair in the scan not excluded by the limits. Green crosses are predicted by the GUT unification scale, early unification is denoted by red crosses, and blue stars are valid for the mirage unification scenario.

From figures 9a,b we see that for $\phi = 0^\circ$, ($\theta = 30^\circ, \theta = 60^\circ$) we require a (3%, 5%) measurement of $m_{\tilde{q}_{avg}}/m_{\tilde{g}}$ and a (11%, 10%) measurement of $m_{\tilde{e}_R}/m_{\tilde{g}}$ to discriminate the three scenarios. In fact, these ratios discriminate for any fixed value of θ, ϕ but do not completely discriminate once the goldstino angles are scanned over. It is therefore difficult to say much that is definitive about the ratios in this case. It is possible that specific models will predict the goldstino angles, and in that case the two ratios mentioned above will be useful. However, the connection between measured quantities and θ, ϕ is perhaps less obvious than for $m_{3/2}$ and $\tan \beta$. This means that it is difficult to see how one would directly infer their values from experimental data, and so we leave the discussion of constrained goldstino angles here.

3.6 Interpretation

Note that the required accuracy quoted here is the one necessary to separate the closest two points between different scenarios, *i.e.* assuming that the data lie within one of the predicted regions, what accuracy would definitely exclude the other two regions. This is the most pessimistic scenario, and we may well require less accuracy depending upon where the data finally lie. For example figure 6a shows that the data $m_{\tilde{d}_L}/m_{\tilde{e}_R} \sim 3.1 \pm 0.6$ and $m_{\tilde{g}}/m_{\tilde{u}_L} \sim 1.05 \pm 0.03$, would imply that the GUT-scale scenario would be selected over the other two whereas for $m_{\tilde{d}_L}/m_{\tilde{e}_R} \sim 1.8$ and $m_{\tilde{g}}/m_{\tilde{u}_L} \sim 1.0$, uncertainties of (0.2, 0.02) would be required respectively. Where the data finally lie will also decide the most important measurement. We take the dilaton dominated scenario to exemplify this point (see figure 7a). If the data lie over the GUT-scale region, the most important errors are those upon $m_{\tilde{e}_L}/m_{\tilde{e}_R}$ as this will best separate the GUT-scale scenario from the other two. If, on the other

hand, the data lie over the early unification scenario, it is more important to have smaller uncertainties upon $m_{\tilde{g}}/m_{\tilde{u}_L}$ for discrimination against the mirage unification scenario.

We must ask what effect theoretical errors have on the interpretation of the results. Comparisons between the spectra derived from **SOFTSUSY** [25] code and **ISASUGRA** [18], while showing qualitative agreement, display differences of order of the mass differences required to discriminate the scenarios [26, 25]. The errors are both dependent upon the flavour of particle (sleptons tend to have very good agreement, whereas coloured objects typically show a 3-5% difference) and on the region of parameter space. For extreme places in parameter space, for example near the radiative electroweak symmetry breaking boundary, predicted mass differences can be large between the two codes [26, 25]. However, provided the point in parameter space being examined is not particularly special, any theoretical errors in codes should not change our conclusions about discrimination. This is because the errors due to (for example) not including finite threshold corrections in **ISASUGRA** will affect all points in the three scenarios in roughly the same way, moving them all in one direction for example. The statistical errors $m_t = 175 \pm 5$ GeV similarly provide an uncertainty. We note that this error should be drastically reduced by Run II of the Tevatron.

It is clear, however, that better accuracy in the mass predictions will be necessary when interpreting real data. Of course, the discrimination depends at face value on the assumption of prior knowledge either of the goldstino angles (which will probably not be owned) or of $m_{3/2}$ and $\tan\beta$. The latter pair of parameters may be predicted in the hypothesis of each scenario, since gaugino masses can help us divine $m_{3/2}$ and $\tan\beta$ may well be obtained from Higgs measurements [24]. We note that each discriminating plot is valid for two particular values of fixed parameters. If the fixed parameters are not determined beforehand, they would have to be fit to the sparticle masses. This fitting procedure will be subject more to the theoretical errors, and will require them to be shrunk from their current levels. We would of course use all available (*i.e.* measured) highly discriminating ratios simultaneously in order to try to pin down the correct scenario. This would provide additional confirmation that the identified scenario is the correct one.

It is likely that the next machine capable of producing TeV-scale superparticles in sufficient numbers to make a reasonable measurement is the LHC. It remains to be seen how good the LHC is in determining ratios of masses, but it cannot constrain any single sparticle mass to a very accurate level (10% or so on the absolute values). The LHC can, however, constrain certain functions of masses to about 1% [27, 28, 7, 29] by finding the end-points of kinematic distributions. In ref. [29], the three most accurate measurements were found to be on the edges in the invariant masses detailed in table 2. They follow parts of the decay chain of $\tilde{q} \rightarrow q\chi_2^0$, $\chi_2^0 \rightarrow l\tilde{l}$, then $\tilde{l} \rightarrow l\chi_1^0$. The existence of this chain depends upon the mass ordering $m_{\tilde{q}} > m_{\chi_2^0} > m_{\tilde{l}}$.

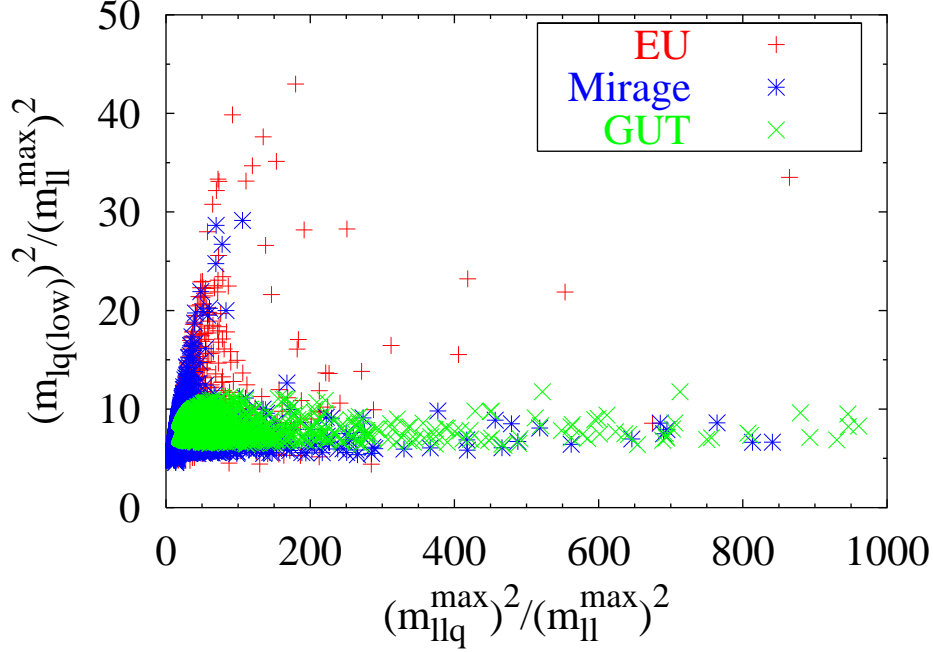


Figure 10: Ratios of LHC edge variables. Each plotted point corresponds to one data point in four-dimensional parameter space $(\theta, \phi, \tan\beta, m_{3/2})$ that is not excluded by the imposed limits and where $m_{\chi_2^0} > m_{\tilde{l}_R}$.

The edges shown in table 2 measure [29]

$$\begin{aligned}
 (m_{ll}^{\max})^2 &= \frac{(m_{\chi_2^0}^2 - m_{\tilde{l}_R}^2)(m_{\tilde{l}_R}^2 - m_{\chi_1^0}^2)}{m_{\tilde{l}_R}^2}, \\
 (m_{lq(\text{low})})^2 &= \min \left[\frac{(m_{\tilde{q}}^2 - m_{\chi_2^0}^2)(m_{\chi_2^0}^2 - m_{\tilde{l}_R}^2)}{m_{\chi_2^0}^2}, \frac{(m_{\tilde{q}}^2 - m_{\chi_2^0}^2)(m_{\tilde{l}_R}^2 - m_{\chi_1^0}^2)}{2m_{\tilde{l}_R}^2 - m_{\chi_1^0}^2} \right], \\
 (m_{llq}^{\max})^2 &= \max \left[\frac{(m_{\tilde{q}}^2 - m_{\chi_2^0}^2)(m_{\chi_2^0}^2 - m_{\chi_1^0}^2)}{m_{\chi_2^0}^2}, \frac{(m_{\tilde{q}}^2 - m_{\tilde{l}_R}^2)(m_{\tilde{l}_R}^2 - m_{\chi_1^0}^2)}{m_{\tilde{l}_R}^2}, \right. \\
 &\quad \left. \frac{(m_{\tilde{l}_R}^2 m_{\tilde{q}}^2 - m_{\chi_1^0}^2 m_{\chi_2^0}^2)(m_{\chi_2^0}^2 - m_{\tilde{l}_R}^2)}{m_{\tilde{l}_R}^2 m_{\chi_2^0}^2} \right], \tag{3.6}
 \end{aligned}$$

except for the special case in which $m_{\tilde{l}_R}^4 < m_{\tilde{q}}^2 m_{\chi_1^0}^2 < m_{\chi_2^0}^4$ and $m_{\chi_2^0}^4 m_{\chi_1^0}^2 < m_{\tilde{q}}^2 m_{\tilde{l}_R}^4$ when $(m_{llq}^{\max})^2 = (m_{\tilde{q}} - m_{\chi_1^0})^2$ instead. We use m_{ll}^{\max} to normalise the other edge variables, as its small error is negligible.

We therefore plot the ratios $(m_{llq}^{\max})^2 / (m_{ll}^{\max})^2$ against $(m_{lq(\text{low})})^2 / (m_{ll}^{\max})^2$ in figure 10 in order to see if these precision LHC measurements can be used to distinguish the string scenarios. All four free parameters are scanned over and all current experimental constraints (including $g - 2$ of the muon) are applied. Additionally,

we require $m_{\chi_2^0} > m_{\tilde{l}_R}$, to make sure that the above mentioned decay chain actually exists. This is the case in roughly one third of the investigated scan points.

edge variable	accuracy
$m_{\tilde{l}}^{\max}$	0.1%
$m_{\tilde{l}q}^{\max}$	1%
$m_{lq(\text{low})}$	1%

Table 2: Accuracy of most useful LHC edge variables.

As figure 10 shows, there is no clear separation between all scenarios on the basis of these LHC edge variables. However, the $(m_{lq(\text{low})})^2/(m_{\tilde{l}}^{\max})^2$ -axis provides some exclusion limits: the GUT scale case could be ruled out if $(m_{lq(\text{low})})^2/(m_{\tilde{l}}^{\max})^2$ does not lie between 7 and 12. The horizontal axis appears to contain no discriminatory power.

4. Conclusions

We have seen that general information can be obtained about string theory scenarios. We considered three general string scenarios: two with the MSSM superfield content (GUT scale unification and mirage unification at the intermediate scale) and one with additional leptons and unification at the intermediate scale. We have mapped out the available parameter space for each scenario, using current empirical constraints.

Our main results are better summarised in figures 3 and 6. Figure 3 provides a map of viable parameter space slices for each of the three scenarios. We can see clearly that for different combinations of values of the goldstino angles different regions of $m_{3/2} - \tan\beta$ parameter space are allowed.

In figure 6 we find that ratios of particle masses may be able to separate each scenario when *all* parameters: $\theta, \phi, m_{3/2}, \tan\beta$ are considered. This allows us to differentiate between the three scenarios provided the data do not appear in certain overlap regions. Clearly, fixing some of the parameters makes the separation between scenarios cleaner (see figs. 7-9). We then determined what accuracy is required on the measurement of these masses in order to distinguish the scenarios. The errors are required to be less than the few percent level, depending upon the exact ratio.

A previous study [30] found that the exotic heavy leptons present in the early unification scenario, can be discovered by the LHC if their masses are less than 980 GeV. This could confirm the mirage scenario, making further discrimination redundant between the models considered here. The exotic leptons would not be discovered if they were heavier than 1 TeV, so all three scenarios would still be left to be distinguished in that case. We note that a previous study confronted a fundamental SUGRA model with detailed linear collider and LHC measurements in a bottom-up approach [31]. Presumably, this kind of analysis could be repeated for stringy scenarios and would complement the present study. It could be used to provide accurate measurements of high-scale soft-breaking parameters and to determine at what scale they unify.

The small percent-level errors required on mass ratios are not expected to occur at the Tevatron experiments [32], or even at the LHC [7]. But it is likely that a

	\tilde{g}	$m_{\tilde{e}_R}$	$m_{\tilde{e}_L}$	$m_{\tilde{u}_L}$	$m_{\tilde{t}_1}$	$m_{\tilde{t}_2}$	$M_{\tilde{\chi}_1^0}$	m_{H^0, A^0}
Early	380	180	230	410	190	450	100	170
Mirage	310	170	210	430	130	450	77	160
GUT	320	160	200	450	180	470	55	190

Table 3: Lower bounds on relevant sparticle masses coming from the parameter scans, in GeV. The rows are marked by string scenario: early unification, mirage and GUT-scale unification respectively.

future linear e^+e^- collider facility [24] would have sufficient accuracy, provided it had sufficient centre of mass energy to produce some of the particles involved in the ratios. For this reason, we present the lower bounds on relevant sparticle masses in table 3 for each scenario. Notice that this is an explicit way to differentiate the different scenarios. If, for instance, the neutralinos are discovered with a mass smaller than 60 GeV this would clearly favour the GUT scenario over the other two. Although the LHC can cover the lower bounds on each sparticle mass, only a multi TeV facility such as CLIC would provide enough centre of mass energy to produce sparticles if their masses are several TeV. We note, however, that lower values of $m_{3/2}$ (and therefore lower sparticle masses) are favoured by the fine-tuning parameter [8].

There are several directions in which our work can be extended. First we may incorporate the charge and colour breaking (CCB) constraints on all the scenarios, as was done for the dilaton domination scenario in ref. [8]. While it would certainly be interesting to know if the universe were in some meta-stable vacuum, a global CCB vacuum might not necessarily rule the model out [33]. We could impose some arbitrary fine-tuning constraint on the models in order to restrict the maximum values of $m_{3/2}$; this would presumably increase the discriminatory power of our mass ratio tests. Another extension relates to the consideration of moduli domination, a limit that we did not consider since in that case the soft breaking terms appear only at the loop level and therefore anomaly mediation cannot be neglected. It is an open question to correctly combine anomaly mediation with gravity mediation for all soft breaking terms.

This study is a crude first step towards the experimental discrimination of string models, leaving plenty of room for more investigation. For example, we only considered two mass ratios at a time for discrimination, but this could be generalised to higher numbers, requiring an automated algorithm for finding the most discriminating ratios. It would be interesting to know the search reach in parameter space of the various future colliders as could be performed by HERWIG [34]. Further, we would like to know under which conditions experiments will be able to measure the discriminatory mass ratios.

We hope that the techniques introduced in this article can be used to discriminate other SUSY breaking scenarios, assuming eventual discovery of supersymmetric

particles.

Acknowledgments

This work is funded by the Studienstiftung des deutschen Volkes and the UK Particle Physics and Astronomy Research Council (PPARC). DG and FQ thank CERN Theory division for their hospitality. DG thanks H Baer for advice on the ISASUGRA package. BCA thanks J Ellis for providing inspiration and we would all like to thank members of the Cambridge LHC SUSY working group for interesting discussions on more experimental aspects.

References

- [1] E. Witten, *Strong Coupling Expansion Of Calabi-Yau Compactification*, *Nucl. Phys.* **B 471** (1996) 135, [[hep-th/9602070](#)].
- [2] K. Benakli, *Phenomenology of Low Quantum Gravity Scale Models*, *Phys. Rev.* **D 60** (1999) 104002, [[hep-ph/9809582](#)].
- [3] C. P. Burgess, L. E. Ibáñez and F. Quevedo, *Strings at the Intermediate Scale, or is the Fermi Scale Dual to the Planck Scale?*, *Phys. Lett.* **B 447** (1999) 257, [[hep-ph/9810535](#)].
- [4] G. Aldazabal, L. E. Ibáñez and F. Quevedo, *Standard-like models with broken supersymmetry from type I string vacua*, *J. High Energy Phys.* **01** (2000) 031, [[hep-th/9909172](#)]; *A D-brane alternative to the MSSM*, *J. High Energy Phys.* **0002** (2000) 015, [[hep-ph/0001083](#)]; D. Bailin, G. V. Kraniotis and A. Love, *Supersymmetric standard models on D-branes*, *Phys. Lett.* **B 502** (2001) 209, [[hep-th/0011289](#)]; G. Aldazabal, L. E. Ibáñez, F. Quevedo and A. M. Uranga, *D-branes at singularities: A bottom-up approach to the string embedding of the standard model*, *J. High Energy Phys.* **0008** (2000) 002, [[hep-th/0005067](#)].
- [5] L. E. Ibáñez, *Mirage gauge coupling unification*, [[hep-ph/9905349](#)].
- [6] A. E. Faraggi, J. S. Hagelin, S. Kelley and D. V. Nanopoulos, *Sparticle spectroscopy*, *Phys. Rev.* **D 45** (1992) 3272; A. Dedes and A. E. Faraggi, *D-term spectroscopy in realistic heterotic-string models*, *Phys. Rev.* **D 62** (2000) 016010, [[hep-ph/9907331](#)].
- [7] ATLAS collaboration, *ATLAS Detector and Physics Performance Technical Design Report*, CERN/LHCC/99-15, ATLAS TDR 14, 25 May 1999.
- [8] S. A. Abel, B. C. Allanach, L. E. Ibáñez, M. Klein and F. Quevedo, *Soft SUSY Breaking, Dilaton Domination and Intermediate Scale String Models*, *J. High Energy Phys.* **12** (2000) 026, [[hep-ph/0005260](#)]; S. A. Abel and B. C. Allanach, *Quasi-Fixed Points and Charge and Colour Breaking in Low Scale Models*, *J. High Energy Phys.* **07** (2000) 037, [[hep-ph/9909448](#)].

- [9] S. Baek, P. Ko and H. S. Lee, *Muon anomalous magnetic moment, $B \rightarrow X/s$ gamma and dark matter detection in the string models with dilaton domination*, *Phys. Rev. D* **65** (2002) 035004, [[hep-ph/0103218](#)]; D. G. Cerdeño, E. Gabrielli, S. Khalil, C. Muñoz and E. Torrente-Lujan, *Muon anomalous magnetic moment in supersymmetric scenarios with an intermediate scale and nonuniversality*, *Phys. Rev. D* **64** (2001) 093012, [[hep-ph/0104242](#)].
- [10] D. Bailin, G. V. Kraniotis and A. Love, *Sparticle spectrum and dark matter in type I string theory with an intermediate scale*, *Phys. Lett. B* **491** (2000) 161, [[hep-ph/0007206](#)].
- [11] E. Gabrielli, S. Khalil, C. Muñoz and E. Torrente-Lujan, *Initial scales, supersymmetric dark matter and variations of neutralino nucleon cross sections*, *Phys. Rev. D* **63** (2001) 025008, [[hep-ph/0006266](#)]; D. G. Cerdeño, E. Gabrielli, S. Khalil, C. Muñoz and E. Torrente-Lujan, *Determination of the string scale in D-brane scenarios and dark matter implications*, *Nucl. Phys. B* **603** (2001) 231, [[hep-ph/0102270](#)].
- [12] J. A. Casas, A. Ibarra and C. Muñoz, *Phenomenological viability of string and M-theory scenarios*, *Nucl. Phys. B* **554** (1999) 67, [[hep-ph/9810266](#)].
- [13] A. Brignole, L. E. Ibáñez and C. Muñoz, *Towards a Theory of Soft Terms for the Supersymmetric Standard Model*, *Nucl. Phys. B* **422** (1994) 125, [[hep-ph/9308271](#)].
- [14] J. A. Bagger, T. Moroi and E. Poppitz, *Anomaly mediation in supergravity theories*, *J. High Energy Phys.* **04** (2000) 009, [[hep-th/9911029](#)].
- [15] M. Cvetič, A. Font, L. E. Ibáñez, D. Lüst and F. Quevedo, *Target space duality, supersymmetry breaking and the stability of classical string vacua*, *Nucl. Phys. B* **361** (1991) 194; L. E. Ibáñez and D. Lüst, *Duality anomaly cancellation, minimal string unification and the effective low-energy Lagrangian of 4-D strings*, *Nucl. Phys. B* **382** (1992) 305, [[hep-th/9202046](#)]; V. S. Kaplunovsky and J. Louis, *Model independent analysis of soft terms in effective supergravity and in string theory*, *Phys. Lett. B* **306** (1993) 269, [[hep-th/9303040](#)].
- [16] H. Baer, M. A. Diaz, P. Quintana and X. Tata, *Impact of physical principles at very high energy scales on the superparticle mass spectrum*, *J. High Energy Phys.* **04** (2000) 016, [[hep-ph/0002245](#)].
- [17] C. H. Chen, M. Drees and J. F. Gunion, *Searching for Invisible and Almost Invisible Particles at e^+e^- Colliders*, *Phys. Rev. Lett.* **76** (1996) 2002, [[hep-ph/9512230](#)], [[Erratum-ibid.](#) **82** (1999) 3192, [hep-ph/9902309](#)]; *A non-standard string/SUSY scenario and its phenomenological implications*, *Phys. Rev. D* **55** (1997) 330, [[hep-ph/9607421](#)], [[Erratum-ibid.](#) **60** (1999) 039901, [hep-ph/9902309](#)].
- [18] H. Baer, F. E. Paige, S. D. Protopopescu and X. Tata, *ISAJET 7.48: A Monte Carlo Event Generator for pp , $\bar{p}p$, and e^+e^- Interactions*, [[hep-ph/0001086](#)].

- [19] Particle Data Group, *Review of Particle Properties*, *Eur. Phys. J. C* **15** (2002) 1, and 2001 partial update for the 2002 edition available on the PDG WWW pages <http://pdg.lbl.gov/>.
- [20] LEPSUSYWG, ALEPH, DELPHI, L3 and OPAL experiments, note LEPSUSYWG/01-03.1 http://lepsusy.web.cern.ch/lepsusy/www/inos_moriond01/charginos_pub.html; and LEPSUSYWG/01-07.1 http://lepsusy.web.cern.ch/lepsusy/www/lsp_cmssm_budapest01/cMSSM_208.html
- [21] H. N. Brown *et al.*, Muon $g - 2$ Collaboration, *Precise measurement of the positive muon anomalous magnetic moment*, *Phys. Rev. Lett.* **86** (2001) 2227, [[hep-ex/0102017](#)].
- [22] S. Narison, *Muon and tau anomalies updated*, *Phys. Lett. B* **513** (2001) 53, [Erratum-*ibid.* **B 526** (2002) 414], [[hep-ph/0103199v5](#)].
- [23] G. Aldazabal, L. E. Ibáñez and F. Quevedo, *A D-Brane Alternative to the MSSM*, *J. High Energy Phys.* **02** (2000) 015, [[hep-ph/0001083](#)].
- [24] ECFA/DESY LC Physics Working Group (J. A. Aguilar-Saavedra *et al.*), *TESLA Technical Design Report Part III: Physics at an $e+e-$ Linear Collider*, [[hep-ph/0106315](#)].
- [25] B. C. Allanach, *SOFTSUSY: a program for calculating supersymmetric spectra*, *Comput. Phys. Commun.* **143** (2002) 305, [[hep-ph/0104145](#)].
- [26] B. C. Allanach, *Theoretical Uncertainties in Sparticle Mass Predictions*, P3-19 preprint of Snowmass **2001** conference, CERN-TH/2001-255, [[hep-ph/0110227](#)].
- [27] I. Hinchliffe, F. E. Paige, M. D. Shapiro, J. Soderqvist and W. Yao, *Precision SUSY measurements at LHC*, *Phys. Rev. D* **55** (1997) 5520, [[hep-ph/9610544](#)].
- [28] J. G. Branson *et al.*, *High transverse momentum physics at the Large Hadron Collider*, [[hep-ph/0110021](#)].
- [29] B. C. Allanach, C. G. Lester, M. A. Parker and B. R. Webber, *Measuring sparticle masses in non-universal string inspired models at the LHC*, *J. High Energy Phys.* **09** (2000) 004, [[hep-ph/0007009](#)].
- [30] B.C. Allanach *et al.*, *Detecting Exotic Heavy Leptons at the Large Hadron Collider*, *J. High Energy Phys.* **08** (2001) 051, [[hep-ph/0108097](#)].
- [31] G. A. Blair, W. Porod and P. M. Zerwas, *Reconstructing supersymmetric theories at high energy scales*, *Phys. Rev. D* **63** (2001) 017703, [[hep-ph/0007107](#)].
- [32] SUGRA Working Group Collaboration (S. Abel *et al.*), *Report of the SUGRA working group for run II of the Tevatron*, [[hep-ph/0003154](#)].

- [33] S.A. Abel and C.A. Savoy, *On metastability in supersymmetric models*, *Nucl. Phys.* **B 532** (1998) 3, [[hep-ph/9803218](#)].
- [34] G. Corcella *et al.*, *HERWIG 6.1 Release Note*, [hep-ph/9912396](#); G. Corcella *et al.*, *HERWIG 6: an event generator for Hadron Emission Reactions With Interfering Gluons (including supersymmetric processes)*, *J. High Energy Phys.* **01** (2001) 010, [[hep-ph/0011363](#)].